Multi experimental and computational studies for DNA and HSA interaction of new nano-scale ultrasound-assisted synthesized Pd(II) complex as a potent anticancer drug

Monireh Dehkhodaei, Mehdi Sahihi, Hadi Amiri Rudbari, Mahnaz Ariaeefar, Sajjad Gharaghani, Reza Azadbakht, Salman Taheri, Abolghasem Abbasi Kajani

Multi experimental and computational studies for DNA and HSA interaction of new nano-scale ultrasound-assisted synthesized Pd(II) complex as a potent anticancer drug

Monireh Dehkhodaei [a], Mehdi Sahihi [a], Hadi Amiri Rudbari [a], Mahnaz Ariaeefar [a], Sajjad Gharaghani [b], Reza Azadbakht [c], Salman Taheri [d], A bolghasem Abbasi Kajani [a]

[a] Department of Chemistry, University of Isfahan, Isfahan 81746-73441, Iran

[b] Laboratory of Bioinformatics and Drug Design (LBD), Institute of Biochemistry and Biophysics, University of Tehran, Tehran, Iran

[c] Department of Chemistry, Payame Noor University, P.O. Box 19395-3697, Iran

[d] Chemistry and Chemical Engineering Research Center of Iran, Tehran, Iran

Abstract

As for daily increasing mortality rate in world due to the growth of cancer causing agents, design and synthesis of new compounds with anticancer potential benefits is one of the most important challenges for researchers. In the present work, we synthesized a new Schiff base Pd(II) complex in bulk-scale and also in nano-scales by Sonochemical method. The structure of synthesized complex was determined by single crystal X-ray diffraction technique. Then the cell viability percent of HeLa cancer cells was studied by MTT assay. The results confirmed that reducing the size has salient effect in annihilation of cancer cells. Also, nano-scale complex reached to IC50 in 10 μM of concentration. Binding ability of the nano- and bulk-scale Pd(II) Schiff base complex with calf thymus DNA and human serum albumin was investigated using combination of experimental (fluorescence, circular dichroism (CD) and viscosity) and computational (molecular docking, molecular dynamics simulation and QM/MM) methods. The estimated binding constants for the complex in both of bulk- and nano-scales showed that the nano-scale complex binds more tightly to DNA than its bulk-scale form. This finding is in good agreement with MTT assay results. Molecular docking studies revealed that Pd(II) complex binds to the minor groove and IB binding site of DNA and HSA, respectively. Also, MD simulation studies showed that complexation with the Pd(II) complex changes the structure of HSA with compared to free protein. Finally, the ONIOM results indicated that the structural parameters of the compound changed along with binding to DNA and HSA, indicating the strong interaction between the compound and these biomacromolecules. The values of binding constants depend on the extent of the resultant changes.

Keywords

Sonochemistry

Nano complex

Fluorescence enhancement

MD simulation

Molecular docking

QM/MM

1. Introduction

Platinum-containing drugs such as cis-platin, carboplatin and oxaliplatin show their anti-cancer activity based on in-vivo interaction with the DNA of the cancerous cells. Studying on the interactions between DNA and the other transition metal complexes is key step to develop new metal based therapeutics [1]. Furthermore, some studies have investigated binding of the anti-cancer drugs to the Human Serum Albumin (HSA), as the most abundant plasma carrier protein in the blood stream [2,3]. The binding ability of a drug to the non-specific transporter protein HSA is an important research field in chemistry, biochemistry and clinical medicine [[4], [5], [6], [7], [8], [9], [10], [11], [12], [13]]. Hence, investigation of the interaction between HSA and small drug molecules is very important for understanding the mystery of life and the interaction mechanisms of drugs. The results of investigation show that more than 90% plasma protein can be combined with metal drugs in form of covalent bonds. Studying on the metal base drugs is one of the basic area in bioinorganic chemistry field. The researchers in this field try to discover compounds with more impressive properties and less side effects from cis-platin that is known as appropriate anti-cancer drug. One of the approaches is using the synergic effect between metals and biological ligands. Schiff bases are the class of inorganic ligands that their biological activities have been proven, previously [[14], [15], [16]]. On the other hand, the simplistic synthesis and wide range of applications of Schiff base ligands have attracted a lot of interests. These compounds play an important role in development of coordination chemistry related to catalysis, organic synthesis [17,18], antitumor, antimicrobial and cytotoxic activity [[19], [20], [21], [22]]. In recent years, remarkable attention has been paid to biological applications of the metal complexes of Schiff bases due to their stability, biocompatibility and biological activity [23,24]. Their biological activity is due to the existence of imine group in their chemical structure [[25], [26], [27]]. Furthermore, complexation of Schiff base ligands with transition metal ions, enhances their biological activities [[28], [29], [30]]. Some palladium complexes had shown promising results as antimalarial and anti-cancer agents in previous investigations [31,32]. Also, due to remarkable similarity between Pd(II) and Pt(II) complexes [33]; and their less toxicity and higher activity in compared to platinum complexes; they are regarded as potential anticancer substances and have better anticancer activity than their Pt(II) analogues in some cases [34].

Due to the importance and significant growth of nanotechnology in all sciences, its role in the field of biology and drug design cannot be ignored. Previous studies showed that the interaction between nanoparticles and biomolecules can change the biomolecule conformation and perturb the normal protein function which can be lead to unexpected biological reactions and toxicity. Therefore, investigation of these types of interactions could not be ignored [35].

Herein, a new Schiff base Pd(II) complex (PdL_2) was synthesized and its molecular structure was determined by single crystal X-ray diffraction technique. The cell viability percent of HeLa cancer cells was first studied by MTT assay. In order to increase the colloidal stability and suitability for the biomedical applications, the nano-scale compound was also synthesized using ultrasound-assisted method and used for in vitro studies. Finally, binding ability of the nano- and bulk-scale PdL_2 with calf thymus DNA (CT-DNA) and HSA was investigated using combination of

experimental (fluorescence, circular dichroism (CD) and viscosity) and computational (molecular docking, molecular dynamics simulation and qm/mm) methods.

2. Experimental section

2.1. Materials sources

All of the used chemicals for synthesis of the complex including 2-amino-propane (Isopropylamine), 2-hydroxybenzaldehyde (salicylaldehyde), triethylamine and Palladium chloride (PdCl2) were purchased from Merck Co. and were used without further purification. All of the used salts for buffer preparation were analytical grade and were dissolved in double distilled water. All of the solutions were used freshly after preparation. Also, HSA, CT-DNA, RPMI-1640 medium, Fetal bovine serum (FBS), Dimethyl sulfoxide (DMSO), antibiotics (penicillin-streptomycin) solution, and 3-(4,5-Dimethylthiazol-2-yl)-2,5-Diphenyltetrazolium Bromide (MTT) were obtained from Sigma- Aldrich.

2.2. Synthesis of the bulk- and nano-scale Pd(II) Schiff base complex (PdL_2)

A methanolic solution (30 ml) of Isopropylamine (IUPAC name: 2-amino-propane) (5 mmol) was added slowly to 30 ml of a methanolic stirred solution of salicylaldehyde (IUPAC name: 2-hydroxybenzaldehyde) (5 mmol) in ambient temperature. The colour immediately changed to yellow and the mixture was then stirred for 2 h. Then a solution of triethylamine (7 mmol) in absolute methanol (10 ml) was added dropwise to ligand solution. The mixture was stirred for 15 min again. Then, a solution of appropriate $PdCl_2$ (2.5 mmol) in methanol (30 ml) was added to the mixture, gently, for synthesis of the complex in bulk-scale. The solution was refluxed overnight to proceed completely. The resulting yellow powder was isolated by filtration and washed by dry methanol several times. Appropriate single crystals for X-ray crystallography were obtained directly from the reaction mixture. In order to prepare the complex in nano scale, a saturated solution was prepared by adding excess powder to 10 ml of DMF at room temperature. The solution was pumped from a small orifice into 100 ml of the antisolvent (water), which was placed in an ultrasonic bath at 180 W for 30 min and was continuously stirred. The suspension was centrifuged at 5000 *g* for 15 min, and the supernatant was withdrawn and filtered through a 0.2 mm pore-size syringe filter [36].

2.3. Single crystal diffraction studies

X-ray data for PdL_2 complex was collected at room temperature with a Bruker APEX II CCD area detector diffractometer using Mo K_α radiation ($k = 0.71073$ Å). Data collections, cell refinements, data reductions and absorption corrections were performed using multiscan methods with Bruker software [[37], [38], [39]]. The structure was solved by direct methods using SIR2004 [40]. The non-hydrogen atoms were refined anisotropically by the full matrix least squares method on F^2 using SHELXL [41]. All hydrogen atoms were added at ideal positions and constrained to ride on their parent atoms. Molecular graphics were prepared with the Olex^2 program [42]. Crystallographic data for complex are listed in Table S1. Selected bond distances and angles are summarized in Table S2.

2.4. Cell viability assay

MTT assay was used to investigate the anticancer potential of the bulk- and nano-scale PdL_2 on human cervical cancer cell line (HeLa) according to the previously reported procedure [43]. The cells were first cultured in RPMI-1640 medium supplemented with 10% FBS and 1% antibiotics solution and were maintained in a humidified 5% CO_2 incubator at 37 °C. When the cell confluence was reached to 70%, the cells were harvested and seeded on 96-well plates at a density of 10^4 cells per well containing 200 µl medium and incubated overnight at the same conditions. After exposure to different concentrations of each compound for 48 h, the medium was removed and 100 µl MTT solution (0.5 $mg \cdot ml^{-1}$ in media) was added into each well and the plates were incubated again at 37 °C for 4 h. The medium was then completely removed and the formazan crystals were dissolved in 150 µl DMSO and the absorbance was measured at 570 nm. Each experiment was conducted in triplicate and the results were presented as the mean values obtained from three independent experiments. The cell viability was determined as ratio of absorbance values from each treatment and the control.

2.5. Preparation of DNA, HSA, bulk- and nano-scale PdL_2 stock solutions for binding experiments

The stock solution of CT-DNA was prepared in 50 mM Tris buffer at pH = 7.5 using double-distilled deionized water and was stored at 4 °C. The CT-DNA concentration per nucleotide was determined using absorption intensity at 260 nm after adequate dilution with the buffer and using the reported molar absorptivity of 6600 $M^{-1} \cdot cm^{-1}$ [44]. Purity of CT-DNA solution was confirmed by ratio of UV absorbance at 260 and 280 nm ($A_{260}/A_{280} = 1.9$), indicating that CT-DNA is free from protein impurity [45]. Also, a stock solution of HSA was prepared by dissolving the desired amount of HSA in 50 mM phosphate buffer (pH = 7). The HSA stock solution was stored at 4 °C in the dark and was used within 2 h. HSA concentration was determined by UV–Vis spectrophotometry using the molar absorption coefficient 35,700 $M^{-1} \cdot cm^{-1}$ at 278 nm [46]. For preparation of PdL_2 solution in bulk-scale, appropriate amounts of obtained complex powder was dissolved in DMSO as co-solvent, and then diluted with corresponding buffer to the required concentration for all experiments. The volume of co-solvent never exceeded 5% (v/v), so the effect of DMSO is negligible. Also, the appropriate amount of the nano-scale PdL_2 powder was dispersed in Tris and phosphate buffer for DNA and HSA binding experiments, respectively.

2.6. Fluorescence spectroscopy measurements

Fluorescence experiments were carried out using quartz cuvette with 1 cm optical path length and the excitation and emission slits were set at 5 and 10 nm, respectively. For investigation of HSA interaction with PdL_2 by this technique, 2 ml of HSA solution was placed into the quartz cell and various amounts of PdL_2 were added to the cell (for both of bulk- and nano-scale). The fluorescence intensities were measured with excitation wavelength at 295 nm and emission wavelength range of 300–450 nm. In each measurement, the mixture was allowed to incubate for 2 min after addition of the compound. Furthermore, all intensities were corrected for the dilution effect in fluorescence experiments. Also, for investigation of interaction between PdL_2 compound and DNA, the CT-DNA solution was stirred with EB with molar ratio of CT-DNA: EB 10:1 and was incubated for 1 h at 4 °C for completion of interaction between CT-DNA and EB. Then, various amounts of PdL_2 compound were added to the mixture of CT-DNA: EB. The fluorescence spectra were measured in the range of 500–700 nm with exciting wavelength at 520 nm. In each measurement after addition of PdL_2, the mixture was incubated for 2 min. Moreover, the measured

fluorescence intensities were corrected for the dilution effect (for both of bulk- and nano-scale). Also, the measured fluorescence intensities were corrected for the inner-filter effect. To eliminate the inner filter effects, absorption measurements were carried out at the fluorescence excitation and emission wavelengths. The extent of this effect can be roughly evaluated with the following relationship: [47]

$$F_{corr} = F_{obs} \times e^{(A_{ex}+A_{em})/2} \quad (1)$$

where, F_{corr} and F_{obs} are the corrected and observed fluorescence intensities, respectively, and Aex and Aem are the absorption of PdL_2 at excitation and emission wavelengths, respectively. All the fluorescence intensities obtained in this study were corrected.

2.7. Circular dichroism spectroscopy

The circular dichroism (CD) spectra were recorded at room temperature using 0.1 cm quartz cell in the near-UV region (190–260 nm) for HSA. The CD spectrum of HSA solution was recorded before and after addition of the nano-scale PdL_2 complex with molar ratio 1:1. The analysis CD of HSA spectra were carried out by CDNN software. The content of secondary conformation of HSA in each step was calculated from this technique.

2.8. Viscosity measurement

Viscosity experiments were carried out using a rotational viscometer and the measurements were performed at 200 rpm at room temperature. The viscosity of CT-DNA solution was measured in the presence of various amounts of the bulk and nano-scale PdL_2. The obtained data are presented as $(\eta/\eta_0)^{1/3}$ versus $[PdL_2]/[\text{CT-DNA}]$, where η and η_0 are viscosity of CT-DNA in the absence and presence of PdL_2, respectively.

3. Computational methods

3.1. Molecular docking calculations

Docking study was carried out to indicate the HSA and DNA-binding site for PdL_2 complex. The 3D structure of PdL_2 was obtained using the .cif file of its X-ray crystal structure. The .cif file was converted to the .pdb format using the Mercury software (http://www.ccdc.cam.ac.uk/). The crystal structures of HSA (PDB ID: 1AO6) and DNA (PDB ID: 423D) with sequence $d(ACCGACGTCGGT)_2$ were taken from the Brookhaven Protein Data Bank (http://www.rcsb.org/pdb). The resolution of these files was 2.5 and 1.6 Å for HSA and DNA, respectively. Water molecules of the .pdb files were deleted, missing hydrogen atoms and Gasteiger charges were added. Flexible ligand docking was carried out by AutoDock 4.2.5.1 molecular docking program using the implemented empirical free energy function and the Lamarckian Genetic Algorithm [48]. The Gasteiger charges were added to prepare the macromolecule input file for docking and the AutoGrid was used to calculate the grids. For docking of the PdL_2 complex to HSA and DNA, a blind docking with 126 lattice points along X, Y, and Z axes was performed to find the binding site of complex on the biomacromolecules. Grid point spacing was set to 0.375 Å, to allow the complex to rotate freely. In the next step, the centre

of the grid box was located at the binding site and the second docking was performed using a cubic box with 60 × 60 × 60 dimensions. 250 docking runs with 25,000,000 energy evaluations for all runs were performed.

3.2. Molecular dynamics (MD) simulation

MD simulation method was used to compare the structural changes of HSA and DNA in the absence and presence of PdL_2 complex. The PdL_2-HSA and PdL_2-DNA complexes with the most negative free binding energy were considered as the initial conformations for the MD studies. GROMACS 5.1.2 package [49] and Amber99 force field [50,51] were used to carry out all MD studies. The partial atomic charges of PdL_2 were calculated using Gaussian 03 [52] at the level of B3LYP/LanL2dz [53], while the other intramolecular force-field parameters were generated with ACPYPE [54] and VFFDT [55] for the organic moiety and the metal center, respectively. Free biomacromolecules and PdL_2-biomacromolecule complexes were located in the cubic box with the periodic boundary conditions in the three directions. The solutes were placed in the center of box and the minimum distance between solute surface and the box was 1.0 nm. The box was filled with TIP3P water molecules [56,57], and the solvated systems were neutralized by adding appropriate amounts of sodium ions (Na^+) and chloride ions (Cl^-). After energy minimization using the steepest descent method, the systems were equilibrated for 200 ps at the temperature of 300 K. Finally, a 10 ns MD simulation was carried out at 1 bar and 300 K. Parrinello-Rahman barostate [58,59] at 1 bar, Berendsen thermostat [60] at 300 K. 9 Å cut off for Van der Walls (VdW) and Coulomb interactions and the particle mesh Ewald (PME) method [61,62] for long range electrostatics were used. The leap-frog algorithm with the 2 fs time step was used to integrate the equation of motions. Finally, an all-bond constrain was used to keep the PdL_2 from drifting and the atomic coordinates were recorded to the trajectory file every 0.5 ps for later analysis.

3.3. QM/MM study

Own N-layered Integrated Molecular Orbital and molecular Mechanics (ONIOM) methodology was employed to carry out QM/MM calculations. The ONIOM can be considered as a hybrid method of quantum mechanical method (QM) with a molecular mechanics (MM). This method is able to apply different ab initio or semi-empirical methods to different parts of a system and combine them to produce reliable geometry and energy at reduced computational time [63]. In the two layers ONIOM method, the total energy (E_{ONIOM}) of the whole system is a sum of the three independent energy calculations: [64].

$$E^{ONIOM\,2} = E^{high}_{model\ system} + E^{low}_{real\ system} - E^{low}_{model\ system} \quad (2)$$

Real system contains full geometry of the molecule and is considered as MM layer while the model system contains the chemically most important (core) part of the system that is considered as QM layer. Furthermore, the stability of respective adducts was obtained by the evaluation the interaction energy (ΔE), which is calculated by the following equation:

$$\Delta E = \Delta E_{Biomacromolecule\ /\ PdL_2} - \Delta E_{Biomacromolecule} - \Delta E_{PdL_2} \quad (3)$$

where $\Delta E_{Biomacromolecule/PdL2}$, $\Delta E_{Biomacromolecule}$ and ΔE_{PdL2} are the energy of the optimized adduct of Biomacromolecule-PdL_2, Biomacromolecule and PdL_2, respectively. Biomacromolecule is HSA or DNA here as receptors. A two layers QM/MM method was used for all calculations. HSA and DNA are considered as low layer while the PdL_2 is considered as high layer in the current work. Molecular mechanics method (UFF) and semi empirical method (PM6) were selected for the low layer and the high layer, respectively.

4. Results and discussion

4.1. Results of experimental sections

4.1.1. PdL_2 synthesis and single crystal X-ray diffraction study

The reaction of the Schiff base ligand with metal ion is shown in Scheme 1A. Also, An ORTEP view of PdL_2 with common atom numbering is shown in Scheme 1B. In the solid state, PdL_2 has a crystallographic center of symmetry that is right in the middle point of the palladium (II) ion in a planar-transoid conformation (Scheme 1B). The molecular unit is centrosymmetric and is made up of equivalent halves. The structure of PdL_2 displays a four coordinate palladium atom coordinated to two bidentate N-isopropylsalicylaldimine anions in a slightly distorted square planer geometry. Each Schiff base ligand acts as a chelate using a phenolato oxygen and an imino nitrogen. The deprotonated isopropylsalicylaldimine ligands are arranged with respect to each other in a trans orientation such that one isopropyl substituent lies above the $[PdO_2N_2]$ plane and

the other below. The Pd O distance [1.9756(15) Å] and the Pd N bond length [2.0368(15) Å] are similar to those were seen in our previous work [65,66]. For instance, distances of 1.982(2)

Å for Pd O bond and 2.017(2) Å for Pd N bond are found in Pd(II) complex with R/S-(1-phenylethylimino)methylnaphtalen-2-ol ligand [66].

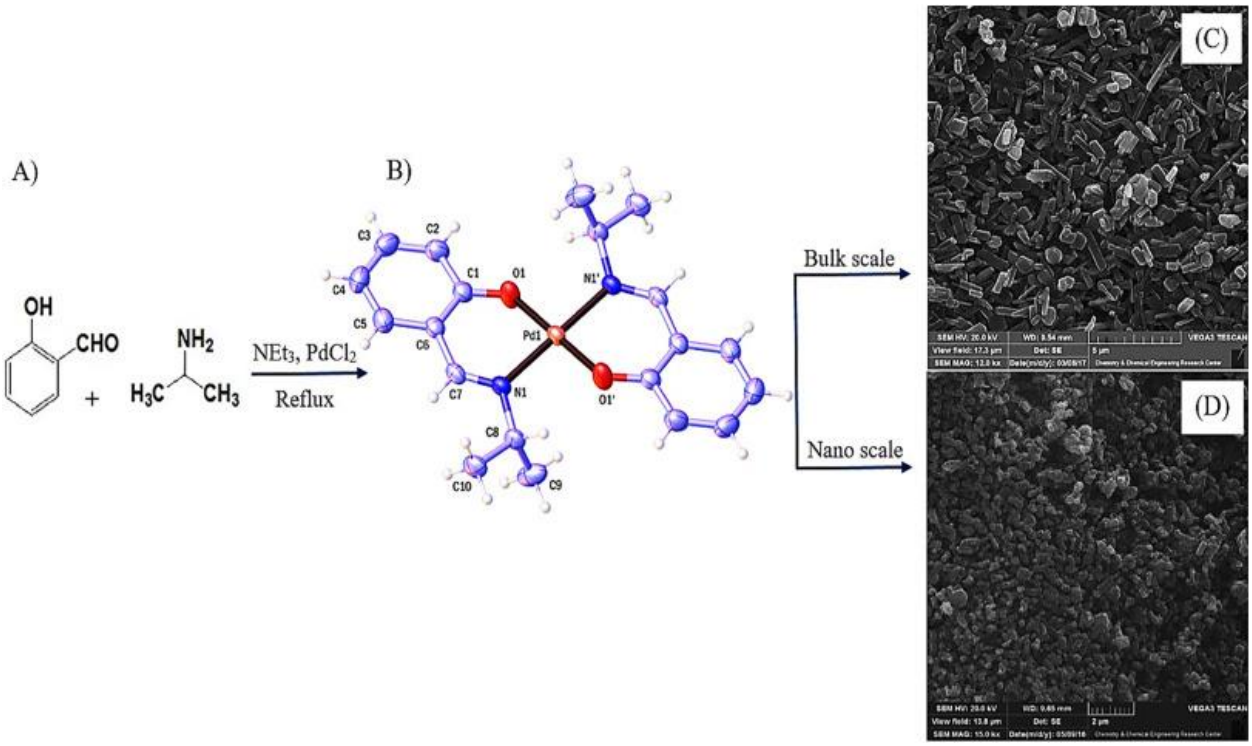

Scheme 1. A) Synthetic routes for preparation of PdL_2. B) ORTEP representation of PdL_2. Displacement ellipsoids are drawn at the 30% probability level and H atoms are shown as small spheres of arbitrary radii. C) SEM image of the bulk-scale PdL_2 complex. D) SEM image of the nano-scale PdL_2 complex.

The C N bond distance is 1.284(3) Å (N1 C7), which is in consistent with a slight elongation of the C N double bond when coordinates to a metal center. Close O Pd N bond angles to 90° [O(1) Pd(1) N(1) = 88.61(6)°; O(1) Pd(1) N(1′) = 91.39(6)°] also confirm the distorted square planer geometry for this complex. The crystallographic data and selected bond lengths and angles are collected in Tables S1–2.

4.1.2. Scanning electron microscopy (SEM) measurements

Scheme 1C and D show the morphology of synthesized particles that were investigated under SEM for bulk- and nano-scale PdL_2, respectively. In Scheme 1C the particles exhibit an approximately filament shape and their particles size distribution is about 500–1000 nm. While, in Scheme 1D the particles have sphere shape and their size distribution is under 200 nm. As it can be seen in Scheme 1C and D, the synthesized nano particles have more uniform distribution than the particles in bulk-scale.

4.1.3. MTT assay

The results of MTT assay after 48 h exposure of HeLa cancer cells to different concentrations of bulk and nano-scale PdL_2 were presented in Fig. 1. Interestingly, the nano-scale PdL_2 displayed potent anticancer activity as more than 35% cell mortality was obtained after exposure to 2.4 μM while increasing the concentration to 10 μM led to more than 53% of cell mortality. In contrast, significant less anticancer activity was observed in the presence of the bulk-scale PdL_2 as only 29.56% mortality was obtained in the presence of 10 μM bulk-scale compound and increasing the concentration to 100 μM was necessary in order to reach the IC_{50} level. The results clearly indicated the higher anticancer activity of nano-scale PdL_2 than bulk-scale one. It seems that decreasing the size of the compound significantly affect its biological activity probably due to its higher bioavailability.

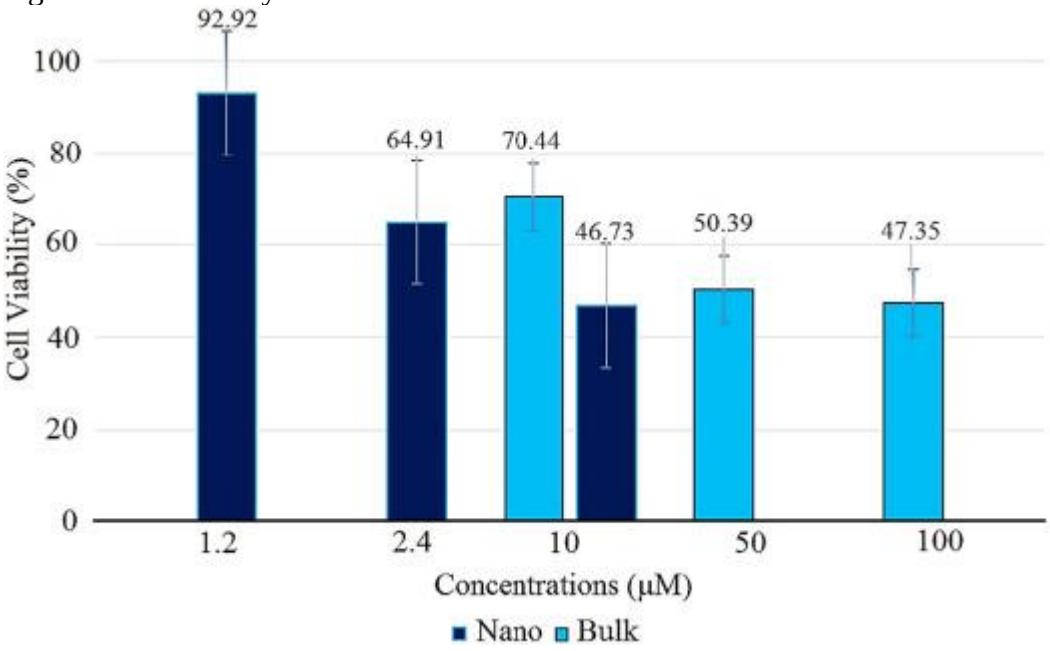

Fig. 1. The viability percentage of HeLa cancer cells after 48 h exposure to different concentrations of bulk- and nano-scale PdL_2.

4.1.4. Fluorescence study for interaction of bulk and nano-scale PdL_2 with CT-DNA and HSA

The fluorescence spectroscopy has been performed as a reliable and sensitive technique to obtain information about interaction between bulk- and nano-complex PdL_2 with CT-DNA and HSA. Fig. 2A and C represent the fluorescence quenching of HSA in the presence of various amount of bulk- and nano-scale PdL_2, respectively. Actually, the observed fluorescence emission of HSA is mainly due to the tryptophan residue. Fig. 2A and C represent that adding the complex in both of scales, leads to changes of microenvironment around the Trp-214 residue in HSA and causes the fluorescence quenching of HSA. This implies the appropriate interaction of the compound with HSA as a carrier protein. The appearance of isosbestic point signifies that equilibrium is established between HSA and the compound and reflects the formation of the ground state complex between them. Scachard equation was used to obtain the binding affinity: [67].

$$Ln\left(\frac{F_0-F}{F}\right)= Ln(K_b)+ nLn\,[Q] \qquad (4)$$

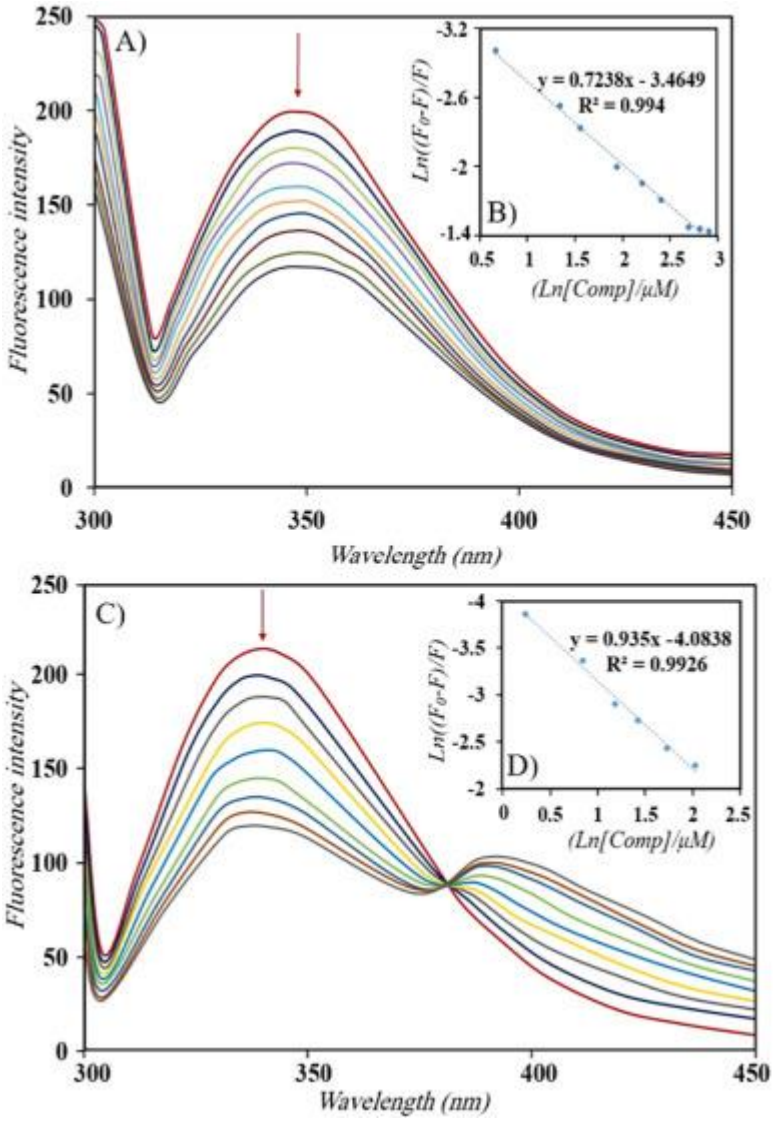

Fig. 2. A) Changes in the fluorescence spectra of HSA in the presence of increasing amounts of bulk-scale PdL_2 in mol ratio of ([HSA]/[PdL_2] = 0–5 ([HSA] = 5 μM, [PdL_2] = 100 μM). B) Plot of Ln((F_0-F)/F) versus Ln[PdL_2]. C) Changes in the fluorescence spectra of HSA in the presence of increasing amounts of nano-scale PdL_2 in mol ratio of ([HSA]/[PdL_2] = 0–5 ([HSA] = 5 μM, [PdL_2] = 25 μM). D) Plot of Ln((F_0-F)/F) versus Ln[PdL_2].

In this equation, F_0 and F are the fluorescence intensity of biomacromolecule in the absence and presence of the compound, respectively. [Q] is the concentration of quencher that quencher is bulk- and nano-scale PdL_2, here. "K_b" is binding constant and is obtained from the plot of $Ln((F_0-F)/F)$ versus Ln [Q] as y-intercept. These plots are shown in Fig. 2B and D. "n" is the number of binding site per biomacromolecule and is determined as slope of the plot. The values of n are nearly 1 for PdL_2 in both of scales indicating the compound binds to HSA with molar ratio of 1:1. The calculated results are presented in Table 1. To determine the interaction mode of the bulk and

nano-scale PdL_2 dispersion with HSA, the Stern–Volmer quenching plots were obtained by monitoring the fluorescence quenching of biomacromolecules with increasing the concentration of the compound according to the Stern–Volmer equation [68]:

$$\frac{F_0}{F} = 1 + K_{sv}[Q] = 1 + k_q \tau [Q] \quad (5)$$

where, F_0 and F are the fluorescence intensity of biomacromolecules in the absence and presence of the compound, respectively. K_{sv} is the Stern-Volmer quenching constant, k_q is the quenching rate constant of biomacromolecules and τ is the average lifetime of biomacromolecules without quencher which is typically equal to 10^{-8} s for biomacromolecules. K_{sv} is determined from the plot of F_0/F vs. [Q] (Fig. S1). Fluorescence quenching is classified as two mechanisms: static quenching and dynamic quenching. In the static mechanism, the fluorophore and the quencher collide together in the ground state while fluorophore and quencher collide together in the excited state in dynamic mechanism. Linearity of the Stern-Volmer plot indicates that fluorescence quenching has only one mechanism: dynamic or static. In this case, if the calculated value of k_q was greater than limiting diffusion rate constant of the diffusional quenching for biopolymers ($2 \times 10^{10}\ M^{-1} \cdot S^{-1}$) support that quenching fluorescence occurs by static mechanism and against that will be dynamic mode.

Table 1. The DNA and HSA-binding constants (K_b), the number of binding sites (n) of the PdL_2.

System	**HSA**		**DNA**	
	K_b **(M^{-1})**	**n**	K_b **(M^{-1})**	**n**
Nano-scale PdL_2	1.68×10^4	0.93	5.59×10^4	0.95
Bulk-scale PdL_2	3.12×10^4	0.72	2.51×10^3	1.18

Here, based on the linearity of Stern-Volmer plot for nano scale (Fig. S1B) and the obtained value of k_q (about $10^{12}\ M^{-1} \cdot S^{-1}$) fluorescence quenching occurs by static mechanism. While, nonlinearity of Stern-Volmer plot for bulk scale Pd-HSA complex indicates that fluorescence quenching is occurred by combination of static and dynamic modes (see Fig. S1A).

On the other hand, investigation of interaction of the compounds with DNA as the first intracellular target for cancer cells is very important. Fig. 3A and C represent the fluorescence enhancement of DNA-Ethidium Bromide (EB) spectrum by adding bulk- and nano-scale PdL_2. The case of fluorescence intensity enhancement that $F > F_0$, the other type of Scachard equation was used to obtain binding constant: [69,70].

$$Ln\left(\frac{F - F_0}{F}\right) = Ln(K_b) + nLn\,[Q] \quad (6)$$

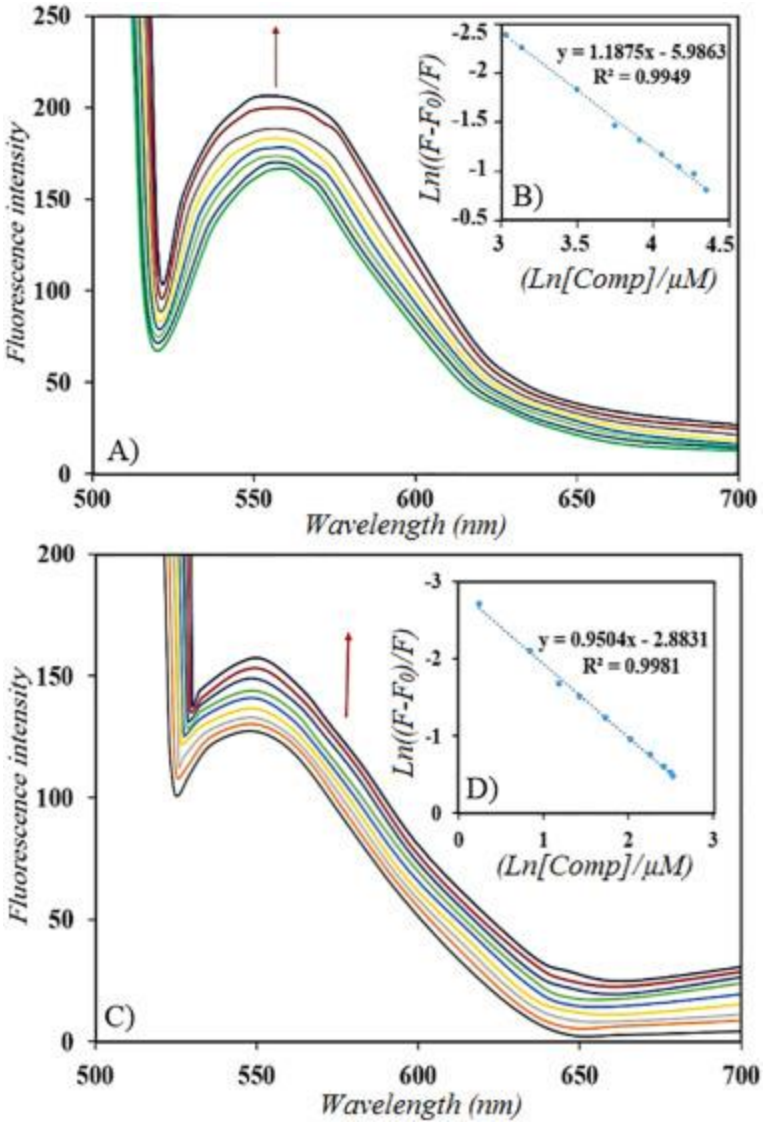

Fig. 3. A) Fluorescence spectra of the EB-DNA in the absence and presence of increasing amounts of bulk-scale PdL_2 in mol ratio of [DNA]/[PdL_2] = 0–5 ([DNA] = 25 μM, [PdL_2] = 250 μM). B) Plot of Ln((F-F_0)/F) versus Ln[PdL_2]. C) Fluorescence spectra of the EB-DNA in the absence and presence of increasing amounts of nano-scale PdL_2 in mol ratio of [DNA]/[PdL_2] = 0–5 ([DNA] = 5 μM, [PdL_2] = 25 μM). D) Plot of Ln((F-F_0)/F) versus Ln[PdL_2].

Plots of Ln*((F-F₀)/F)* versus Ln[PdL_2] for obtaining the binding affinity (K_b) of the compound to CT-DNA and the number of binding sites on CT-DNA are present in Fig. 3B and D. The results obtained are collected in Table 1. The values of n for PdL_2 on CT-DNA is similar to HSA and is nearly 1. It means that the compound binds to CT-DNA with molar ratio of 1:1 (see Table 1). The obtained K_b values indicate that PdL_2 in its nano-scale interacts stronger than its bulk-scale to CT-DNA. However, the effect of its size on interaction with HSA is negligible.

To determine the interaction mode of the bulk and nano-scale PdL_2 dispersion with DNA, the F/F_0 vs. [E] plots were obtained by monitoring the fluorescence enhancement of biomacromolecules with increasing the concentration of the compound according to the following equation [71]:

$$\frac{F}{F_0} = 1 + K_E[\mathrm{E}] \quad (7)$$

where, F_0 and F are the fluorescence intensity of biomacromolecules in the absence and presence of the compound, respectively. K_E is the enhancement rate constant of biomacromolecules. K_E is determined from the plot of F/F_0 vs. [E] (Fig. S1).

4.1.5. Circular dichroism study

The CD spectra of HSA in free and bonded to nano-scale PdL_2 complex states are shown in Fig. 4. The CD spectrum of HSA indicates two negative peaks at 208 and 222 nm which are characteristic absorption peaks of α-helical structure of protein attributed to the n-π* transfer for the bonds of the α-helix [52,53]. According to Fig. 4, the intensity of HSA peak has been altered slightly due to the binding of nano-complex. This observation was confirmed by CDNN software analysis for protein secondary structure contents (Fig. 4).

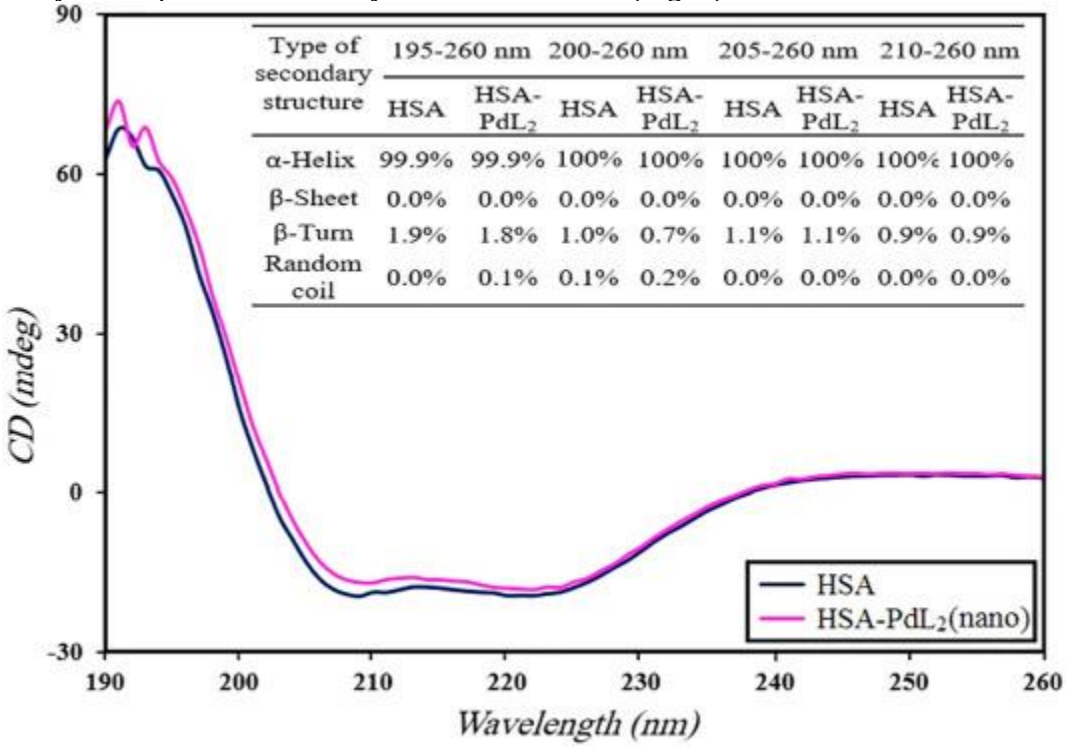

Fig. 4. The CD spectra of HSA in the absence and presence of nano-scale PdL_2 complex in the molar ratio of [Complex]/[HSA] = 1 and the results of CDNN software analysis contents of protein secondary structure.

4.1.6. Viscosity measurement

To further verify the interaction mode of the bulk- and nano-scale PdL_2 with CT-DNA, viscosity measurements of CT-DNA upon addition of the bulk- and nano-scale PdL_2 were carried out. A classical intercalative mode causes an increase in the DNA viscosity due to increasing of overall length of DNA [66]. On the other hand, groove binding and electrostatic interactions could bend the DNA helix, reduce its length and cause the reduction or no change in the DNA viscosity [66].

According to Fig. S2, the viscosity of CT-DNA decreased until molar ratio of $[PdL_2]/[DNA] = 0.3$ and 1.2 in the presence of bulk- and nano-scale PdL_2, respectively and remained constant afterward. The observed trends confirmed that the binding mode of PdL_2 in its both of scales, may be groove binding.

4.2. Results of computational sections

4.2.1. Molecular docking studies

Molecular docking is a virtual powerful tool for drug design. This computational technique helps researchers to predict and obtain first insight about stable structure of receptor-ligand complex. In order to find out the preferred location of the compound on DNA and HSA, molecular docking studies were carried out. The results of molecular docking for interaction of PdL_2 and HSA indicate that the compound is situated in the IB subdomain that is known as third drug binding site of HSA. HSA acts as a carrier for drugs such as Bilirubin, Lidocaine, Indomethacin, Hemin and so on. These drugs bind to IB subdomain of HSA and transfer in body [72]. Fig. 5A represents the location of PdL_2 and its related cluster during its interaction with HSA. The standard binding free energy ($\Delta G°$) of this interaction is about $-8.08\ kcal \cdot mol^{-1}$. This score is related to the docking cluster with maximum population and minimum binding energy (see Fig. 5A). Furthermore, intermolecular energy which covers H-bonding interactions, Van der Walls, desolvation and electrostatic energies [39], was estimated as $-8.63\ kcal \cdot mol^{-1}$. The amino acids residues with major role in the stability of PdL_2-HSA system are exhibited in Fig. 5A. Also, the docked model in Fig. 5B for PdL_2-DNA system suggests that PdL_2 binds in the minor groove of DNA with $\Delta G°$ and intermolecular energy of -5.48 and $-6.03\ kcal \cdot mol^{-1}$, respectively. These energies are related to docking conformation (1–1) which has maximum population and minimum binding energy. This result is in good agreement with obtained results of viscosity measurements.

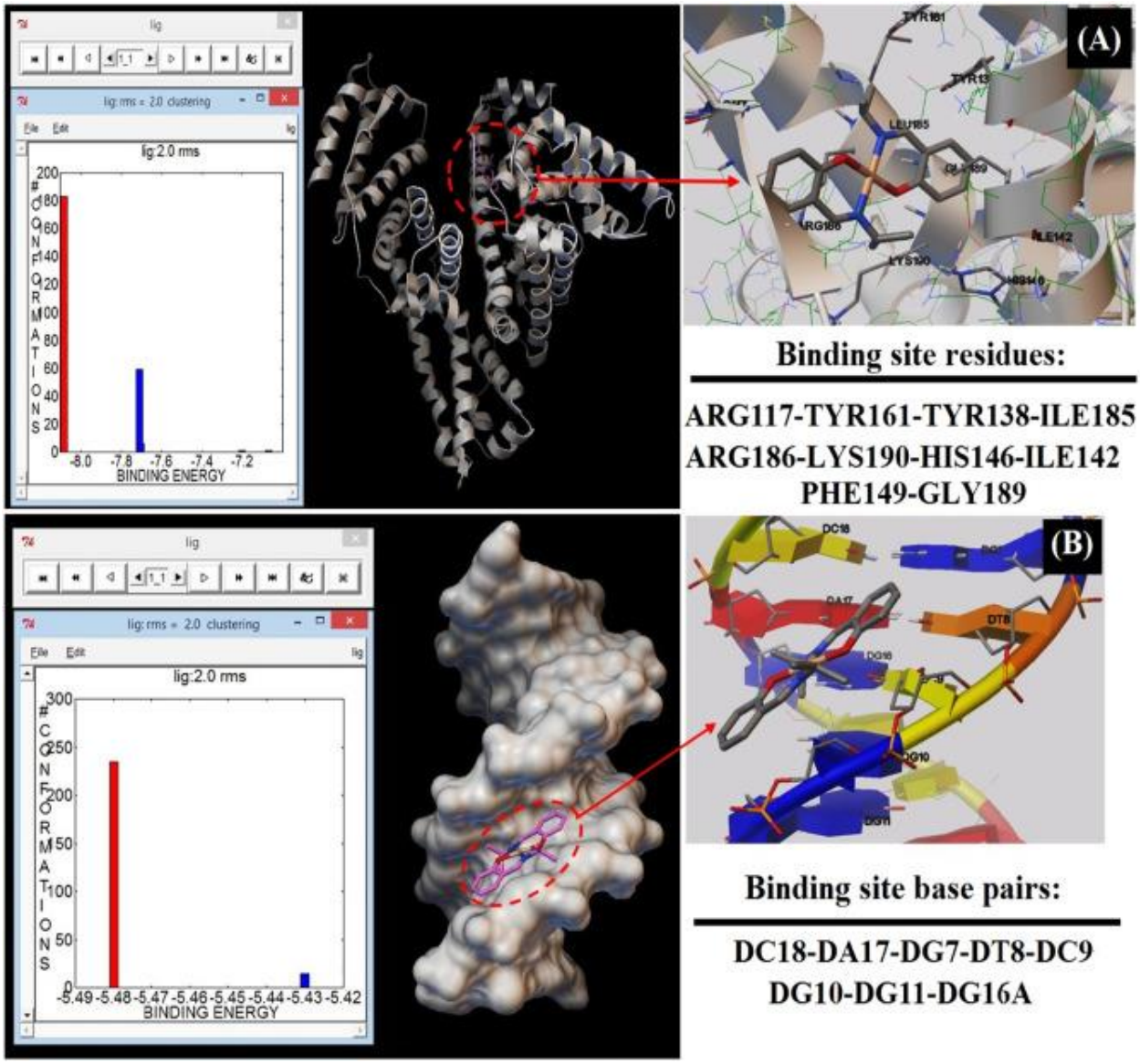

Fig. 5. (A) Location of PdL_2 in its interaction with HSA, the amino acids residues of HSA in binding site and its docking clusters. (B) Location of PdL_2 in its interaction with DNA, the base pairs of DNA in binding site and its docking clusters.

Fig. 5B represents the base pairs of DNA around of PdL_2 complex. Also, molecular docking results shows that H-bond or π stacking interactions have not key role in the stability of DNA- or HSA-PdL_2 systems and the nature of these interactions are mainly hydrophobic.

4.2.2. Molecular dynamics simulation

One of the exact computational approaches for investigation of interaction details between biomacromolecules and small molecules is molecular dynamics (MD) simulation. MD simulation studies for PdL_2 complex with DNA and HSA were carried out and the beginning structures for the MD analyses were selected from the conformations with lowest docking energies. The stability of the system (biomacromolecule and compound) properties was examined by means of RMS

deviations (RMSD) of unbound and ligand conjugated biomacromolecule with respect to the initial structure, RMS fluctuations (RMSF), the solvent accessible surface area (SASA) of biomacromolecule, radius of gyration (Rg) and number of H-bonds. Preliminary simulations over 10 ns time were performed on DNA and HSA with PdL_2. Table 2 provides the average values of RMSD, SASA, Rg and number of H-bonds of the HSA, HSA-PdL_2, DNA and DNA-PdL_2 systems. Fig. 6 represents time dependence of RMSD, Rg, H-bond and RMSF values of HSA and HSA-PdL_2 systems. Fig. 6A indicates that the trajectories of both systems are stable and their RMSD reached equilibrium and fluctuated around its mean value after about 5 ns simulation time. Figs. 6B and S3 show that complexation with PdL_2 changed the structure of HSA with compared to free protein. It can be clearly seen that the Rg was smaller upon binding of the PdL_2 suggesting a more compact structure of HSA in the presence of PdL_2. Decreasing the number of intramolecular H-bonds is another evidence that confirms a modified structure of HSA in the presence of PdL_2 (Fig. 6C). Also, local protein mobility was analyzed by calculating the time averaged RMSF values of free HSA and HSA-PdL_2 complex and was plotted against residue numbers based on the last 5000 ps trajectory (Fig. 6D). The profiles of atomic fluctuations were found to be very similar to those of free HSA and HSA-PdL_2 complex. RMSF highlights the conformational adjustments of the protein structure, in conjunction with PdL_2 conformational adaptation to its binding sites. The results indicate that the residues that were in contact with the PdL_2 are stable and have low RMSF values suggesting that the structure of drug binding site remains rigid during simulation. Hence, it can be concluded that the interactions of protein and PdL_2 were stable during the simulation time. Fig. 7 represents time dependence of RMSD and RMSF values of DNA and DNA-PdL_2 systems. Fig. 7A indicates that the trajectories of both systems are stable and their RMSDs reach equilibrium and fluctuate around their mean values after about 1 ns simulation time. Also, local DNA mobility was analyzed by calculating the time averaged RMSF values of free DNA and DNA-PdL_2 complex and was plotted against atom numbers based on the last 8000 ps trajectory (Fig. 7B). The results indicate that the atoms of DNA bound PdL_2 are stable and have lower RMSF values than the free DNA. Hence, it can be concluded that the interactions of DNA and PdL_2 were stable during the simulation time.

Table 2. The average values of RMS deviation (RMSD), number of H-bonds, the radius of gyration (R_g) and the solvent accessible surface area (SASA) of the HSA, HSA-PdL_2, DNA and DNA-PdL_2 systems.

System	RMSD (nm)	H-bond	Rg (nm)	SASA (nm^2)
HSA	0.26 ± 0.05	481.5 ± 10.9	2.70 ± 0.02	298.22 ± 3.71
HSA + PdL_2	0.25 ± 0.03	470.0 ± 10.9	2.68 ± 0.01	299.00 ± 5.61
DNA	0.25 ± 0.10	33.14 ± 1.48	–	–
DNA + PdL_2	0.25 ± 0.12	33.17 ± 1.72	–	–

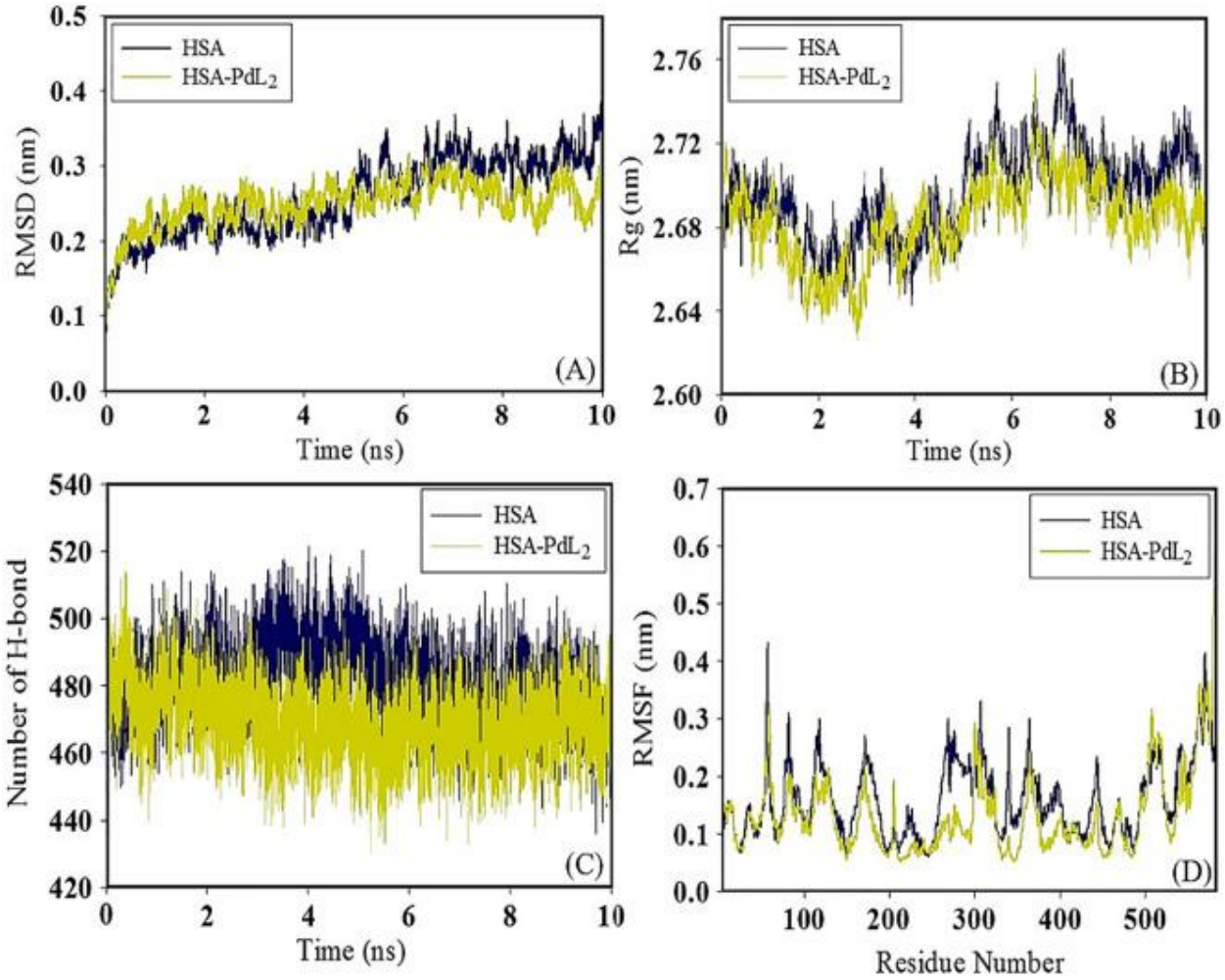

Fig. 6. (A) Time dependence of RMSD. RMSD values for HSA and HSA-PdL_2 complex during 10 ns MD simulation. (B) Time-evolution of radius of gyration (Rg) for HSA and HSA-PdL_2 complex during 10 ns MD simulation. (C) The number of Intramolecular H-bonds for HSA and HSA-PdL_2 complex during 10 ns MD simulation. (D) RMSF values of HSA and HSA-PdL_2 complex plotted against residue numbers.

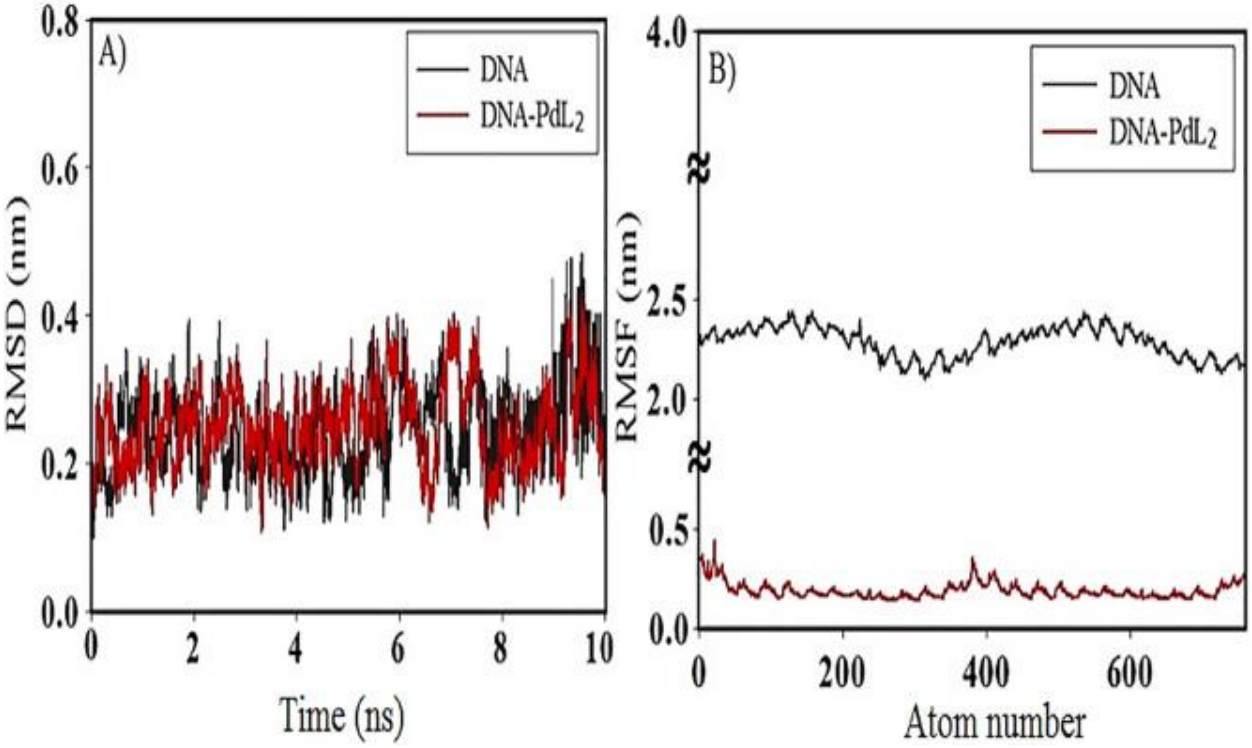

Fig. 7. A) Time dependence of RMSD. RMSD values for DNA and DNA-PdL_2 complex during 10 ns MD simulation. B) RMSF values of DNA and DNA-PdL_2 complex plotted against atom numbers.

4.2.3. QM/MM studies

In this work a two-layer ONIOM calculations including (PM6: UFF) were employed to perform QM/MM studies. The molecular mechanics (MM) was described using the UFF force field for HSA and DNA (low layer) while semi-empirical quantum mechanics (QM) method (PM6) was chosen for the PdL_2 (high layer). The most stable geometries obtained from the molecular docking calculations were opted as starting points of HSA- and DNA-PdL_2 for the two layer ONIOM studies. All calculations were performed using Gaussian 03 quantum chemistry package. The partial atomic charges on the atoms of the PdL_2, DNA and HSA were considered to reoptimize the optimized geometries. The Van der Waals and electrostatic interaction were considered in structure optimization. Moreover, the polarization of the wave function of the PdL_2 was considered to obtain more truthful geometries. The results of ONIOM calculations represented that structure of the PdL_2 deviates from its initial geometry due to binding to HSA and DNA. Along with the interaction of PdL_2 with biomacromolecules some bond lengths and bond angles are changed. Such the changes can be indicative of the strength of the interaction between biomacromolecules and PdL_2. Fig. 8, Fig. 9 show the changes take place in some geometrical parameters including bond angles of PdL_2 along with binding to HSA and DNA. Also, Fig. 9 shows that the distances between the nucleotides were changed due to DNA interaction with PdL_2 complex. The calculated binding energies (ΔE_{ONIOM}) of PdL_2 are 4853.58 and -2883.28 kcal·mol^{-1} for HSA and DNA, respectively. In view of considering the polarization of the PdL_2 in electrostatic field of HSA and

DNA in QM/MM calculation, this energy is more accurate than calculated energy by molecular docking method.

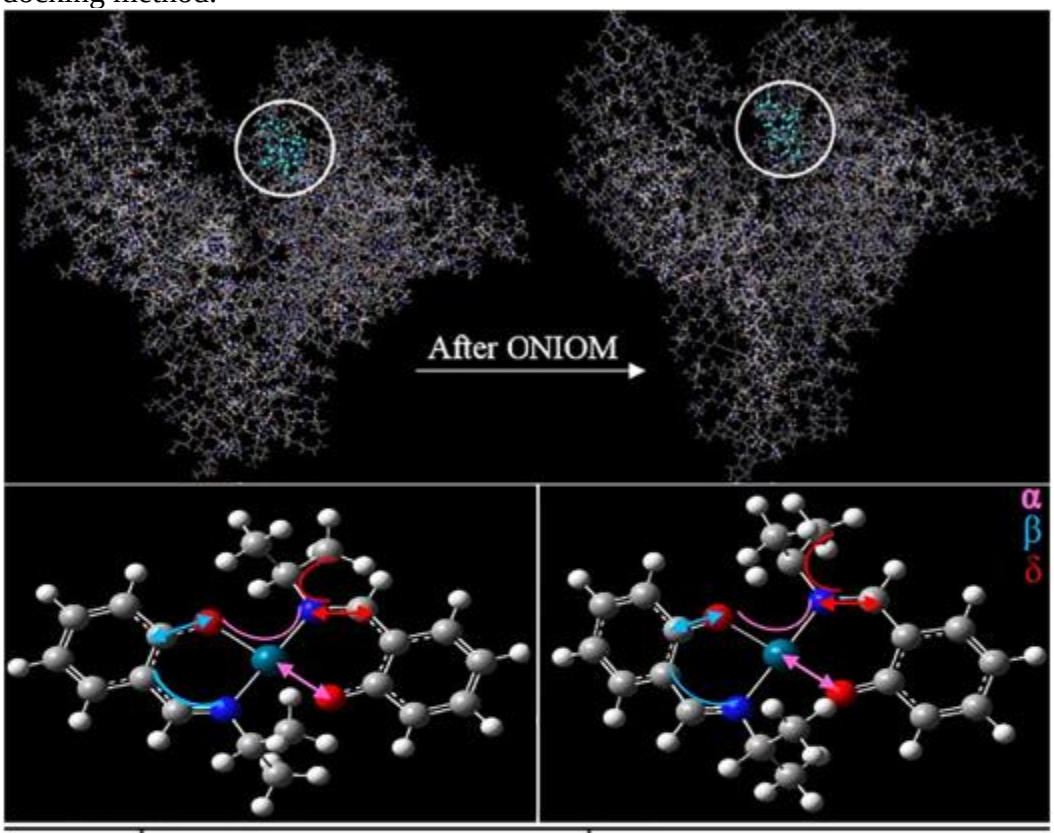

Type of Symbol	(before ONIOM)		(after ONIOM)	
	Angle/Degree	Length (Å)	Angle/Degree	Length (Å)
α	88.66	1.97	91.22	1.99
β	127.90	1.30	123.13	1.28
γ	108.86	1.28	115.24	1.30

Fig. 8. The structure of the PdL_2 complex and HSA optimized considering charged embedding of MM part in QM part in the gas phase (The blue part of system considers as QM part). The changes of structural parameters of PdL_2 during binding to HSA (Arcs and double arrow show angle and length of bond, respectively).

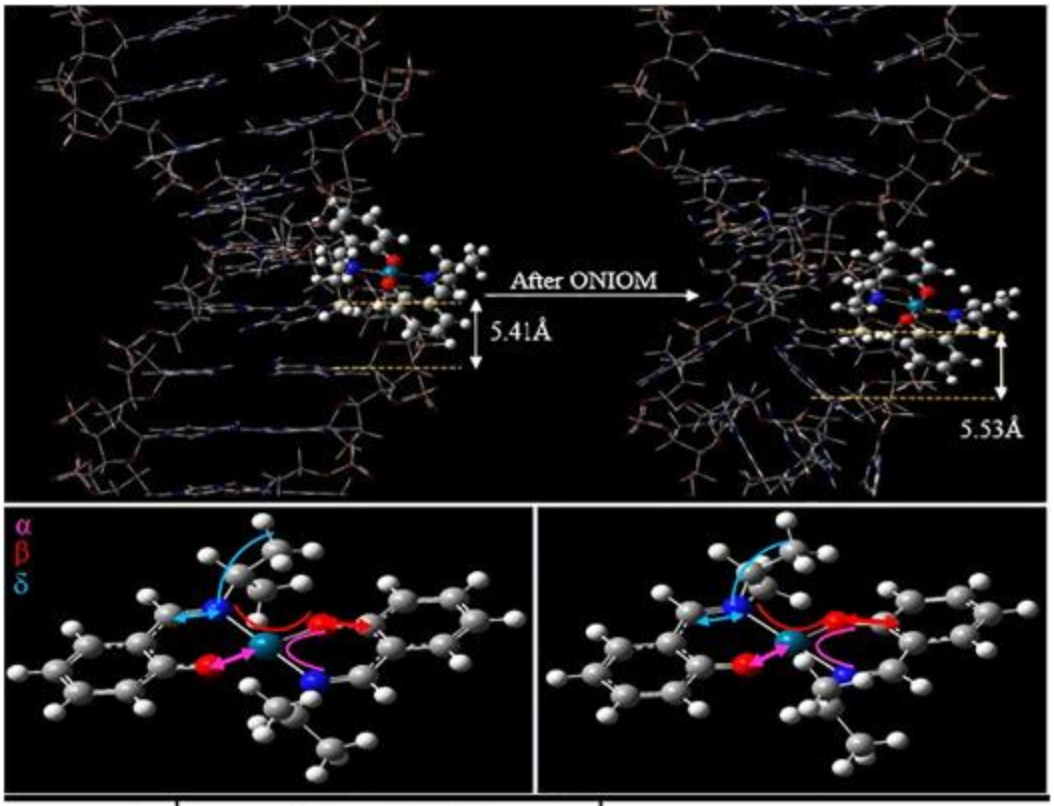

Type of Symbol	(before ONIOM)		(after ONIOM)	
	Angle/Degree	Length (Å)	Angle/Degree	Length (Å)
α	90.95	1.97	91.40	1.98
β	90.90	1.30	88.60	1.27
γ	108.88	1.28	115.21	1.30

Fig. 9. The structure of the PdL_2 complex and DNA optimized considering charged embedding of MM part in QM part in the gas phase. The changes of structural parameters of PdL_2 during binding to DNA (Arcs and double arrow show angle and length of bond, respectively).

5. Conclusion

Here, synthesis of novel Pd(II) complex in bulk and nano scales using ultrasonic waves was described. The structure of complex was established by single crystal X-ray diffraction. The MMT assay results indicated that the anticancer activity of the compound is affected by its size and notable point is that nano-scale complex reached to IC50 in 10 μM of concentration. Investigation of binding affinity, type of interactions and probable changing structure due to interaction of PdL_2 with HSA and DNA, for both of bulk and nano scales complex were carried out by versatile experimental (Fluorescence spectroscopy, viscosity measurement, CD spectroscopy) and computational techniques (molecular docking, ONIOM and MD simulation). According to the obtained results of binding experiments, it can be found that the size decreasing has positive effect

on the binding affinity. Circular dichroism spectroscopy was used to investigate the changes on the secondary structure of HSA upon its interaction with the complex. The existence of slight changing in the HSA peak intensity indicated that the secondary structure of protein has been altered slightly due to the binding of complex. The molecular docking studies exhibited that hydrophobic interaction have a dominant role in the stability of complex-HSA and DNA systems and PdL_2 bind to the minor groove of DNA and IB-binding site of protein. MD simulation and ONIOM studies revealed that conformation of the complex and the biomacromolecules changed due to the strong interaction between the compound and these biomacromolecules.

Acknowledgements

The financial supports of the research council of University of Isfahan are gratefully acknowledged.

Supplementary data

CCDC 1554815 contain the supplementary crystallographic data for PdL2. These data can be obtained free of charge via http://www.ccdc. cam.ac.uk/conts/retrieving.html, or from the Cambridge Crystallographic Data Centre, 12 Union Road, Cambridge CB2 1EZ, UK. Fax: +44 1223 336 033; or e-mail:deposit@ccdc.cam.ac.uk. Supplementary data to this article can be found online at doi: https://doi.org/10. 1016/j.molliq.2018.05.077

References

[1] V.Mahalingam, N. Chitrapriya, F.R. Fronczek, K. Natarajan, Dimethyl sulfoxide ruthenium (II) complexes of thiosemicarbazones and semicarbazone: synthesis, characterization and biological studies, Polyhedron 27 (2008) 2743–2750.

[2] I. Khosravi, F. Hosseini, M. Khorshidifard, M. Sahihi, H.A. Rudbari, Synthesis, characterization, crystal structure and HSA binding of two new N, O, O-donor Schiff-base ligands derived from dihydroxybenzaldehyde and tert-butylamine, J. Mol. Struct. 1119 (2016) 373–384.

[3] A. Ray, B.K. Seth, U. Pal, S. Basu, Nickel (II)-Schiff base complex recognizing domain II of bovine and human serum albumin: spectroscopic and docking studies, Spectrochim. Acta A Mol. Biomol. Spectrosc. 92 (2012) 164–174.

[4] A. Belatik, S. Hotchandani, J. Bariyanga, H. Tajmir-Riahi, Binding sites of retinol and retinoic acid with serum albumins, Eur. J. Med. Chem. 48 (2012) 114–123.

[5] O. Dömötör, S. Aicher, M. Schmidlehner, M.S. Novak, A. Roller, M.A. Jakupec, W. Kandioller, C.G. Hartinger, B.K. Keppler, É.A. Enyedy, Antitumor pentamethylcyclopentadienyl rhodium complexes ofmaltol and allomaltol: synthesis, solution speciation and bioactivity, J. Inorg. Biochem. 134 (2014) 57–65.

[6] B. Bakaeean, M. Kabiri, H. Iranfar, M.R. Saberi, J. Chamani, Binding effect of common ions to human serum albumin in the presence of norfloxacin: investigation with spectroscopic and zeta potential approaches, J. Solut. Chem. 41 (2012) 1777–1801.

[7] J. Chamani, A. Moosavi-Movahedi, O. Rajabi, M. Gharanfoli, M. Momen-Heravi, G. Hakimelahi, A. Neamati-Baghsiah, A. Varasteh, Cooperative α-helix formation of β-lactoglobulin induced by sodium n-alkyl sulfates, J. Colloid Interface Sci. 293 (2006) 52–60.

[8] J. Chamani, A. Moosavi-Movahedi, A. Saboury, M. Gharanfoli, G. Hakimelahi, Calorimetric indication of the molten globule-like state of cytochrome c induced by nalkyl sulfates at low concentrations, J. Chem. Thermodyn. 35 (2003) 199–207.
[9] S. Hamed-Akbari Tousi,M. Reza Saberi, J. Chamani, Comparing the interaction of cyclophosphamide monohydrate to human serum albumin as opposed to holotransferrin by spectroscopic andmolecularmodeling methods: evidence for allocating the binding site, Protein Pept. Lett. 17 (2010) 1524–1535.
[10] S. Marouzi, A.S. Rad, S. Beigoli, P.T. Baghaee, R.A. Darban, J. Chamani, Study on effect of lomefloxacin on human holo-transferrin in the presence of essential and nonessential amino acids: spectroscopic and molecular modeling approaches, Int. J. Biol. Macromol. 97 (2017) 688–699.
[11] Z. Omidvar, A. Asoodeh, J. Chamani, Studies on the antagonistic behavior between cyclophosphamide hydrochloride and aspirin with human serum albumin: timeresolved fluorescence spectroscopy and isothermal titration calorimetry, J. Solut. Chem. 42 (2013) 1005–1017.
[12] S. Rashidipour, S. Naeeminejad, J. Chamani, Study of the interaction between DNP and DIDS with human hemoglobin as binary and ternary systems: spectroscopic and molecular modeling investigation, J. Biomol. Struct. Dyn. 34 (2016) 57–77.
[13] Z. Sharif-Barfeh, S. Beigoli, S. Marouzi, A.S. Rad, A. Asoodeh, J. Chamani, Multispectroscopic and HPLC studies of the interaction between estradiol and cyclophosphamide with human serum albumin: binary and ternary systems, J. Solut. Chem. 46 (2017) 488–504.
[14] M. Dehkhodaei, M. Sahihi, H. Amiri Rudbari, Spectroscopic and molecular docking studies on the interaction of Pd (II) & Co (II) Schiff base complexes with β-lactoglobulin as a carrier protein, J. Biomol. Struct. Dyn. (2017) 1–7.
[15] M. Dehkhodaei, M. Sahihi, H.A. Rudbari, S. Gharaghani, R. Azadbakht, S. Taheri, A.A. Kajani, Studies of DNA-and HSA-binding properties of new nano-scale green synthesized Ni (II) complex as anticancer agent using spectroscopic methods, viscosity measurement, molecular docking, MD simulation and QM/MM, J. Mol. Liq. 248 (2017) 24–35.
[16] M. Dehkhodaei, M. Sahihi, H.A. Rudbari, F. Momenbeik, DNA and HSA interaction of Vanadium (IV), Copper (II), and Zinc (II) complexes derived from an asymmetric bidentate Schiff-base ligand: multi spectroscopic, viscosity measurements, molecular docking, and ONIOM studies, J. Biol. Inorg. Chem. 23 (2018) 181–192.
[17] R. Antony, S.T. David, K. Saravanan, K. Karuppasamy, S. Balakumar, Synthesis, spectrochemical characterisation and catalytic activity of transition metal complexes derived fromSchiff basemodified chitosan, Spectrochim. Acta A Mol. Biomol. Spectrosc. 103 (2013) 423–430.
[18] T. Rosu, E. Pahontu,M. Reka-Stefana, D.-C. Ilies, R. Georgescu, S. Shova, A. Gulea, Synthesis, structural and spectral studies of Cu (II) and V (IV) complexes of a novel Schiff base derived from pyridoxal. Antimicrobial activity, Polyhedron 31 (2012) 352–360.
[19] H.F.A. El-halim, M. Omar, G.G. Mohamed, Synthesis, structural, thermal studies and

biological activity of a tridentate Schiff base ligand and their transition metal complexes, Spectrochim. Acta A Mol. Biomol. Spectrosc. 78 (2011) 36–44.
[20] S.A. Patil, S.N. Unki, A.D. Kulkarni, V.H. Naik, U. Kamble, P.S. Badami, Spectroscopic, in vitro antibacterial, and antifungal studies of Co (II), Ni (II), and Cu (II) complexes with 4-chloro-3-coumarinaldehyde Schiff bases, J. Coord. Chem. 64 (2011) 323–336.
[21] K. Singh, Y. Kumar, P. Puri, M. Kumar, C. Sharma, Cobalt, nickel, copper and zinc complexes with 1, 3-diphenyl-1H-pyrazole-4-carboxaldehyde Schiff bases: antimicrobial, spectroscopic, thermal and fluorescence studies, Eur. J. Med. Chem. 52 (2012) 313–321.
[22] Z.-L. You, D.-H. Shi, C. Xu, Q. Zhang, H.-L. Zhu, Schiff base transitionmetal complexes as novel inhibitors of xanthine oxidase, Eur. J. Med. Chem. 43 (2008) 862–871.
[23] F. Arjmand, F. Sayeed, M. Muddassir, Synthesis of new chiral heterocyclic Schiff base modulated Cu (II)/Zn (II) complexes: their comparative binding studies with CTDNA, mononucleotides and cleavage activity, J. Photochem. Photobiol. B Biol. 103 (2011) 166–179.
[24] N. Pravin, N. Raman, Investigation of in vitro anticancer and DNA strap interactions in live cells using carboplatin type Cu (II) and Zn (II) metalloinsertors, Eur. J. Med. Chem. 85 (2014) 675–687.
[25] R. Antony, S.T.D.Manickam, K. Saravanan, K. Karuppasamy, S. Balakumar, Synthesis, spectroscopic and catalytic studies of Cu (II), Co (II) and Ni (II) complexes immobilized on Schiff base modified chitosan, J. Mol. Struct. 1050 (2013) 53–60.
[26] Z. Guo, R. Xing, S. Liu, Z. Zhong, X. Ji, L. Wang, P. Li, Antifungal properties of Schiff bases of chitosan, N-substituted chitosan and quaternized chitosan, Carbohydr. Res. 342 (2007) 1329–1332.
[27] N. Raman, A. Selvan, S. Sudharsan, Metallation of ethylenediamine based Schiff base with biologically active Cu (II), Ni (II) and Zn (II) ions: synthesis, spectroscopic characterization, electrochemical behaviour, DNA binding, photonuclease activity and in vitro antimicrobial efficacy, Spectrochim. Acta A Mol. Biomol. Spectrosc. 79 (2011) 873–883.
[28] J. Anacona, J.L. Rodriguez, J. Camus, Synthesis, characterization and antibacterial activity of a Schiff base derived from cephalexin and sulphathiazole and its transition metal complexes, Spectrochim. Acta A Mol. Biomol. Spectrosc. 129 (2014) 96–102.
[29] M. Sundararajan, T. Jeyakumar, J. Anandakumaran, B.K. Selvan, Synthesis of metal complexes involving Schiff base ligand with methylenedioxy moiety: spectral, thermal, XRD and antimicrobial studies, Spectrochim. Acta AMol. Biomol. Spectrosc. 131 (2014) 82–93.
[30] A. Tarushi, E. Polatoglou, J. Kljun, I. Turel, G. Psomas, D.P. Kessissoglou, Interaction of Zn (II) with quinolone drugs: structure and biological evaluation, Dalton Trans. 40 (2011) 9461–9473.
[31] P. Chellan, N. Shunmoogam-Gounden, D.T. Hendricks, J. Gut, P.J. Rosenthal, C. Lategan, P.J. Smith, K. Chibale, G.S. Smith, Synthesis, structure and in vitro biological screening of palladium (II) complexes of functionalised salicylaldimine thiosemicarbazones as antimalarial and anticancer agents, Eur. J. Inorg. Chem. 2010 (2010) 3520–3528.
[32] R. Prabhakaran, S. Renukadevi, R. Karvembu, R. Huang, J. Mautz, G. Huttner, R. Subashkumar, K. Natarajan, Structural and biological studies of mononuclear palladium

(II) complexes containing N-substituted thiosemicarbazones, Eur. J. Med. Chem. 43 (2008) 268–273.
[33] A.A. Shoukry, R.M. Alghanmi, Synthesis, DNA binding and complex formation reactions of 3-amino-5, 6-dimethyl-1, 2, 4-triazine with Pd (II) and some selected biorelevant ligands, Spectrochim. Acta A Mol. Biomol. Spectrosc. 138 (2015) 932–941.
[34] A.R. Kapdi, I.J. Fairlamb, Anti-cancer palladium complexes: a focus on PdX 2 L 2, palladacycles and related complexes, Chem. Soc. Rev. 43 (2014) 4751–4777.
[35] L. Calzolai, F. Franchini, D. Gilliland, F. Rossi, Protein − nanoparticle interaction: identification of the ubiquitin − gold nanoparticle interaction site, Nano Lett. 10 (2010) 3101–3105.
[36] R. Azadbakht, J. Khanabadi, A novel aluminum-sensitive fluorescent nanochemosensor based on naphthalene macrocyclic derivative, Tetrahedron 69 (2013) 3206–3211.
[37] A. Bruker, Inc., Madison, Wisconsin, USA,© 2005, COSMO (Version 1.48), SAINT (Version 7.06 A), SADABS.
[38] A. Bruker, Inc., Madison, Wisconsin, USA,© 2005, SAINT (Version 7.06 A), SADABS.
[39] C. Li, J.-X. Wang, Y. Le, J.-F. Chen, Studies of Bicalutamide–excipients interaction by combination of molecular docking and molecular dynamics simulation, Mol. Pharm. 10 (2013) 2362–2369.
[40] M.C. Burla, R. Caliandro, M. Camalli, B. Carrozzini, G.L. Cascarano, L. De Caro, C. Giacovazzo, G. Polidori, R. Spagna, SIR2004: an improved tool for crystal structure determination and refinement, J. Appl. Crystallogr. 38 (2005) 381–388.
[41] G. Sheldrick, SHELXL-97; University of Göttingen: Göttingen, Germany, 1997, There is No Corresponding Record for This Reference, 2010.
[42] O.V. Dolomanov, L.J. Bourhis, R.J. Gildea, J.A. Howard, H. Puschmann, OLEX2: a complete structure solution, refinement and analysis program, J. Appl. Crystallogr. 42 (2009) 339–341.
[43] A.A. Kajani, A.-K. Bordbar, S.H.Z. Esfahani, A. Razmjou, Gold nanoparticles as potent anticancer agent: green synthesis, characterization, and in vitro study, RSC Adv. 6 (2016) 63973–63983.
[44] M. Reichmann, S. Rice, C. Thomas, P. Doty, A further examination of the molecular weight and size of desoxypentose nucleic acid, J. Am. Chem. Soc. 76 (1954) 3047–3053.
[45] K. Zheng, F. Liu, X.M. Xu, Y.-T. Li, Z.Y.Wu, C.-W. Yan, Synthesis, structure and molecular docking studies of dicopper (II) complexes bridged by N-phenolato-N′-[2-(dimethylamino) ethyl] oxamide: the influence of terminal ligands on cytotoxicity and reactivity towards DNA and protein BSA, New J. Chem. 38 (2014) 2964–2978.
[46] C.N. Pace, F. Vajdos, L. Fee, G. Grimsley, T. Gray, How to measure and predict the molar absorption coefficient of a protein, Protein Sci. 4 (1995) 2411–2423.
[47] B.C. MacDonald, S.J. Lvin, H. Patterson, Correction of fluorescence inner filter effects and the partitioning of pyrene to dissolved organic carbon, Anal. Chim. Acta 338 (1997) 155–162.
[48] G.M. Morris, D.S. Goodsell, R.S. Halliday, R. Huey, W.E. Hart, R.K. Belew, A.J. Olson, Automated docking using a Lamarckian genetic algorithm and an empirical binding free energy function, J. Comput. Chem. 19 (1998) 1639–1662.

[49] H.J. Berendsen, D. van der Spoel, R. van Drunen, GROMACS: a message-passing parallel molecular dynamics implementation, Comput. Phys. Commun. 91 (1995) 43–56.
[50] A. Pérez, I. Marchán, D. Svozil, J. Sponer, T.E. Cheatham, C.A. Laughton, M. Orozco, Refinement of the AMBER force field for nucleic acids: improving the description of α/γ conformers, Biophys. J. 92 (2007) 3817–3829.
[51] J.Wang, R.M.Wolf, J.W. Caldwell, P.A. Kollman, D.A. Case, Development and testing of a general amber force field, J. Comput. Chem. 25 (2004) 1157–1174.
[52] A. Frisch, Gaussian 03. U. User's Reference: Manual Version 7.1 (Correspondending to Gaussian 03 Revision D. 1), Gaussian, 2005.
[53] C. Lee,W. Yang, R.G. Parr, Development of the Colle-Salvetti correlation-energy formula into a functional of the electron density, Phys. Rev. B 37 (1988) 785.
[54] A.W.S. da Silva, W.F. Vranken, ACPYPE - antechamber python parser interface, BMC Res. Notes 5 (2012) 367.
[55] S. Zheng, Q. Tang, J. He, S. Du, S. Xu, C.Wang, Y. Xu, F. Lin, VFFDT: a new software for preparing AMBER force field parameters for metal-containing molecular systems, J. Chem. Inf. Model. 56 (2016) 811–818.
[56] W.L. Jorgensen, J. Chandrasekhar, J.D. Madura, R.W. Impey,M.L. Klein, Comparison of simple potential functions for simulating liquid water, J. Chem. Phys. 79 (1983) 926–935.
[57] P. Mark, L. Nilsson, Structure and dynamics of the TIP3P, SPC, and SPC/E water models at 298 K, J. Phys. Chem. A 105 (2001) 9954–9960.
[58] M. Parrinello, A. Rahman, Polymorphic transitions in single crystals: a new molecular dynamics method, J. Appl. Phys. 52 (1981) 7182–7190.
[59] A. Rahman, F.H. Stillinger, Molecular dynamics study of liquid water, J. Chem. Phys. 55 (1971) 3336–3359.
[60] A. Lemak, N. Balabaev, On the Berendsen thermostat, Mol. Simul. 13 (1994) 177–187.
[61] T. Darden, D. York, L. Pedersen, Particle mesh Ewald: an N· log (N) method for Ewald sums in large systems, J. Chem. Phys. 98 (1993) 10089–10092.
[62] U. Essmann, L. Perera, M.L. Berkowitz, T. Darden, H. Lee, L.G. Pedersen, A smooth particle mesh Ewald method, J. Chem. Phys. 103 (1995) 8577–8593.
[63] H. Farrokhpour, H. Hadadzadeh, F. Darabi, F. Abyar, H.A. Rudbari, T. Ahmadi-Bagheri, A rare dihydroxo copper (II) complex with ciprofloxacin; a combined experimental and ONIOM computational study of the interaction of the complex with DNA and BSA, RSC Adv. 4 (2014) 35390–35404.
[64] T. Vreven, K.S. Byun, I. Komáromi, S. Dapprich, J.A. Montgomery Jr, K. Morokuma, M.J. Frisch, Combining quantum mechanics methods with molecular mechanics methods in ONIOM, J. Chem. Theory Comput. 2 (2006) 815–826.
[65] Z. Kazemi, H.A. Rudbari,M. Sahihi, V. Mirkhani, M. Moghadam, S. Tangestaninejad, I. Mohammadpoor-Baltork, S. Gharaghani, Synthesis, characterization and biological application of four novel metal-Schiff base complexes derived from allylamine and their interactions with human serum albumin: experimental, molecular docking and ONIOM computational study, J. Photochem. Photobiol. B Biol. 162 (2016) 448–462.
[66] Z. Kazemi, H.A. Rudbari,M. Sahihi, V. Mirkhani, M. Moghadam, S. Tangestaninejad, I.

Mohammadpoor-Baltork, G. Azimi, S. Gharaghani, A.A. Kajani, Synthesis, characterization and separation of chiral and achiral diastereomers of Schiff base Pd (II) complex: a comparative study of their DNA-and HSA-binding, J. Photochem. Photobiol. B Biol. 163 (2016) 246–260.
[67] J.R. Lakowicz, Plasmonics in biology and plasmon-controlled fluorescence, Plasmonics 1 (2006) 5–33.
[68] H. Boaz, G. Rollefson, The quenching of fluorescence. Deviations from the Stern-Volmer law, J. Am. Chem. Soc. 72 (1950) 3435–3443.
[69] N. Shahabadi, S. Kashanian, F. Darabi, In vitro study of DNA interaction with a watersoluble dinitrogen Schiff base, DNA Cell Biol. 28 (2009) 589–596.
[70] S.U. Rehman, Z. Yaseen,M.A. Husain, T. Sarwar, H.M. Ishqi,M. Tabish, Interaction of 6 mercaptopurine with calf thymus DNA–deciphering the bindingmode and photoinduced DNA damage, PLoS One 9 (2014), e93913. .
[71] P. Anger, P. Bharadwaj, L. Novotny, Enhancement and quenching of single-molecule fluorescence, Phys. Rev. Lett. 96 (2006), 113002. .
[72] A. Varshney, P. Sen, E. Ahmad, M. Rehan, N. Subbarao, R.H. Khan, Ligand binding strategies of human serum albumin: how can the cargo be utilized? Chirality 22 (2010) 77–87.